FULL PAPER

Rapid Fabrication of an Inverse Opal TiO$_2$ Photoelectrode for DSSC Using a Binary Mixture of TiO$_2$ Nanoparticles and Polymer Microspheres

Young Gon Seo, Kyoungja Woo, Junkyung Kim, Hyunjung Lee,* and Wonmok Lee*

A rapid fabrication method of highly reflective TiO$_2$ inverse opal (IO) film exhibiting controllable thickness, high TiO$_2$ content, and excellent interfacial contact with glass substrate is presented. By inducing accelerated solvent evaporation during the colloidal self-assembly process, a composite film of polystyrene (PS)/TiO$_2$ has been directly fabricated on a fluorine doped tin oxide (FTO) glass substrate, which exhibits the highly ordered opaline structure of PS embedded into the TiO$_2$ matrix. This hybrid fabrication path leads to the formation of layers with the preferred {111} face-centered cubic (FCC) orientation parallel to the substrate and to produce a 1 cm^2-wide well-ordered composite colloidal crystal film in less than 30 min. The film showed highly ordered FCC structure, particularly at the upper region, due to the induced solvent evaporation and exhibited a reliable light modulation at a reflectance mode. Regardless of the size of sacrificial PS microspheres, TiO$_2$ IO films of controllable thickness were successfully formed by varying the moving speed of the fabrication cell. The binary aqueous dispersion of tailor-made anatase TiO$_2$ nanoparticles and monodisperse PS microspheres showed a high degree of dispersion stability under basic conditions. Hydrothermal treatment of the TiO$_2$ dispersion favored the crystallinity of the coated film and provided small volume contraction after thermal calcinations. The high degree of dispersion stability enabled to increase TiO$_2$ content in a binary mixture, which is more favorable toward the robust and large-area IO film. The calcined films exhibited excellent mechanical robustness and intimate interfacial contact with the glass substrate. which in turn resulted in higher TiO$_2$ content near the glass substrate. The TiO$_2$ IO film was tested as a dye-sensitized solar cell (DSSC) photoelectrode, and a single cell showed a relatively high photon-to-current conversion efficiency of 4.2%. The high TiO$_2$ content of IO film and its good adhesion to the FTO subratrate remarkably improved in the performance of the solar cell compared to the previous investigations where post-infiltration of TiO$_2$ had been employed.

1. Introduction

Due to unique properties such as photo-activity, crystalline TiO$_2$ nanoparticles have found a wide variety of applications such as in photocatalysis,[1,2] electrocatalysis,[3] antibacterial coatings,[4] sensors,[2,5] and solar cells.[6,7] In particular, thin films of crystalline TiO$_2$ deposited on a transparent conducting oxide (TCO) layer can be directly employed as the photoelectrode for DSSCs.[8,9] In particular, a nanoporous TiO$_2$ film is necessary to achieve the high efficiency that is required in solar cell applications. A highly ordered porous TiO$_2$ film is gaining increasing interest due to its three-dimensional (3D) periodic structure and the relatively high refractive index contrast between TiO$_2$ and the ambient air. More specifically, depending on the periodic size and shape of its 3D structure, a photonic band gap in the visible wavelength range can be obtained.[10–12] Thus, TiO$_2$ films with ordered pore structure are regarded as a promising material platform for photonic crystal devices.[13] The preferred method to fabricate highly ordered TiO$_2$ structures is the infiltration of nanocrystalline TiO$_2$ networks within a self-assembled synthetic opal template. The colloidal template is subsequently etched off by means of either a thermal or a chemical method, and the resulting porous material is characterized as "inverse opal" (IO) since its pore structure follows the original shape of the synthetic

Y. G. Seo, Prof. W. Lee
Department of Chemistry
Sejong University
98 Gunja-dong, Gwangjin-gu, Seoul 143–747, Republic of Korea
E-mail: wonmoklee@sejong.ac.kr
Prof. H. Lee
School of Advanced Materials Engineering
Kookmin University
861–1 Jeongneung-Dong, Seoul, 136–702, Republic of Korea
E-mail: hyunjung@kookmin.ac.kr

Dr. K. Woo
Nano-Materials Center
Korea Institute of Science and Technology
P.O. Box 131, Cheongryang, Seoul, 130–650, Republic of Korea
Dr. J. Kim
Hybrid Polymer Materials Research Center
Korea Institute of Science and Technology
39–1 Hawolgok-dong Seongbuk-gu Seoul, 130–650, Republic of Korea

Materials
Views
www.MaterialsViews.com

ADVANCED
FUNCTIONAL
MATERIALS
www.afm-journal.de

FULL PAPER

opal template. Generally, a highly crystalline TiO_2 structure can be obtained when, assisted by capillary forces, an organometallic titanium (Ti) precursor filling is placed into the interstices of a preformed colloidal crystal template and subsequently, a sol–gel reaction takes place on the TiO_2 structure.[14–16] It has been recently reported that the sol–gel process can also be induced electrochemically, thus the templated electrodeposition can generate TiO_2 photonic crystals.[17,18] Nonetheless, a critical drawback of sol–gel condensation within a colloidal template is the volume contraction of the calcined TiO_2 film due to inevitable loss of the reaction byproducts. As a result, the final TiO_2 film either contains a substantial number of cracks, or becomes completely delaminated from the substrate. Only recently has a dry infiltration process, such as the atmospheric pressure chemical vapor deposition (APCVD),[19] been used in place of the wet coating method. Although adhesion between TiO_2 and substrate has been improved, this new method suffers from significant volume shrinkage (>30%) during the thermally induced phase transformation from amorphous TiO_2 to anatase. Moreover, dry processing is disadvantageous from the view point of the manufacturing cost, as it requires high vacuum conditions and dedicated instrumentation. To overcome the volume shrinkage problem faced with the more economical wet processing, we recently reported on the direct infiltration of nanocrystalline TiO_2 into the colloidal crystal template.[9] In this previous study, organically modified TiO_2 nanocrystals of relatively small size (~5 nm) and narrow size distribution were infiltrated within the interstitial spaces of submicrometer-sized colloidal templates on a FTO glass substrate, and through a post-calcination treatment, a porous DSSC photoelectrode was produced with a reduced number of cracks. The superior quality of the TiO_2 IO photoelectrode was confirmed by its unprecedented photon-to-current conversion efficiency in a single DSSC test. However, several cycles of coating and equal number of drying steps were required before dense enough TiO_2 films could be obtained. Furthermore, the final TiO_2 IO film tended to break when the PS microsphere size becomes as small as 300 nm, because of the difficulties encountered with the infiltration of TiO_2 through the narrow channels between PS microspheres all the way down to the glass substrate. For the TiO_2 IO film to be used as a DSSC photoelectrode, intimate contact between the TiO_2 mesostructure and the TCO layer is a prerequisite, otherwise electron transport through the TiO_2/TCO interface cannot be easily achieved. Taking into account the inherent drawbacks of the infiltration approach, an attractive alternative for the fabrication TiO_2 IO films would be the simultaneous assembly of TiO_2 nanoparticles and the template-generating microspheres.[11,12] The simultaneous coating of the TiO_2 nanoparticles and microspheres also possesses multiple advantages. For example, it can reduce the number of processing steps. Moreover, the contact between TiO_2 and the substrate will be more intimate thanks to the direct coating of TiO_2 deposited on the substrate. Recently, Meng et al. had fabricated a composite PS/TiO_2 film by dip-coating PS microspheres and TiO_2 nanocrystals on a glass substrate.[12] For the fabrication of this well-ordered PS opal film with TiO_2 nanoparticles filling the interstitial spaces, more than 24 h were required. The film after thermal calcination showed a photonic stop-band, rendering it suitable for Bragg diffraction of visible light. However, mixed crystalline facets of {100} and

{111} were observed parallel to the glass substrate as a result of the slow dip coating process.[12]

In the present paper, we report on the rapid (~within 30 min) fabrication of a composite PS/TiO_2 film and the following TiO_2 IO films focused to practical applications, particularly as DSSC photoelectrodes. Various control parameters of the homogeneous dispersion of TiO_2 nanoparticles are considered as well as on the mechanical and optical properties of the high quality TiO_2 IO films with a well-defined FCC structure. Lastly, we investigate the performance of the thermally calcined TiO_2 films deposited on a FTO glass when used as a DSSC photoelectrode.

2. Results and Discussion

2.1. Rapid Fabrication of a Composite Colloidal Crystal Film from PS Microspheres and TiO_2 Nanoparticles

One of the most important outcomes of the present investigation is the rapid formation of a high quality composite colloidal crystal film from PS microspheres and TiO_2 nanoparticles, which is assisted by accelerated water evaporation. The individual steps of this hybrid fabrication process for a TiO_2 IO film is illustrated in **Figure 1**. As the top cell moves along the thin spacers which have been lined one after the other, the binary dispersion of PS microspheres and TiO_2 nanoparticles is deposited on the bottom substrate. Subsequently, the hot air blown from a nozzle which is located 5 cm above the deposited film accelerates the evaporation of water out from the wet film, eventually driving the self-assembly of the PS microspheres into a colloidal crystal film with FCC structure. During the colloidal crystallization process, the homogeneous dispersion of TiO_2 nanoparticles behaves as a uniform dispersing medium for the PS microspheres. Meanwhile, the concentration of the nanoparticles in the drying film gradually increases. An aqueous dispersion of non-aggregated anatase TiO_2 nanoparticle is the key material for the successful deposition of the composite TiO_2/PS films. (see the Supporting Information, Figure S1) In a previous paper, we have shown that an aqueous dispersion of nanocrystalline TiO_2 forms a uniform and transparent film upon spin coating.[20] A highly stable suspension tailor-made anatase TiO_2 nanocrystals in water can be attained by base-catalyzed peptization, followed by a hydrothermal treatment.[10] Thanks to the high crystallinity of the TiO_2 nanoparticles, the refractive index of the spin-coated TiO_2 film was as high as 2.0 without thermal calcinations, and more importantly, the film was almost free from the cracks which are a serious drawback of conventional sol–gel processed titania systems.[4,8] The effect of hydrothermal process on the quality of the final composite film will be discussed later in this paper.

To ensure the stability of the TiO_2 dispersion, we investigated the surface charge of the TiO_2 nanoparticles against pH variations. The home-made TiO_2 nanoparticles were prepared by peptization using tetramethylammonium hydroxide (TMAH) as the basic peptizing agent. The pH of the TiO_2 dispersion was maintained at 8–10 after washing. The basic pH keeps the TiO_2 nanoparticles stable in water by allowing them to carry negative surface charges, so that they repel each other electrostatically.

ADVANCED
FUNCTIONAL
MATERIALS
www.afm-journal.de

FULL PAPER

www.MaterialsViews.com
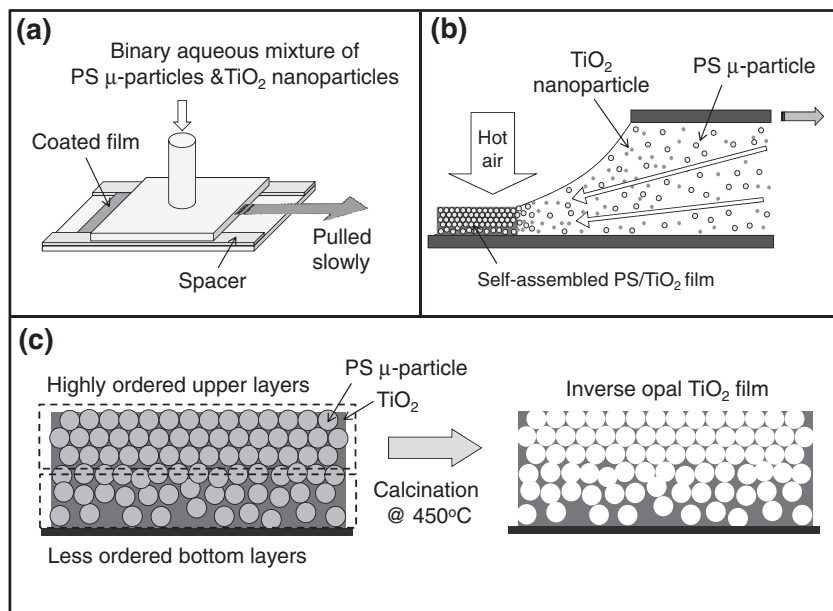
Figure 1. Schematic illustration of the deposition of the binary aqueous dispersion of TiO$_2$ nanoparticles and PS microspheres on a slide glass. a) Experimental set-up. The binary dispersion is supplied from the top cell which is subsequently moved at a constant speed of 0.5–8 mm/min, while bottom substrate remains fixed. b) Side view of a slide coated colloidal self assembly. The evaporation of water is accelerated by means of hot air blown from a slit-like nozzle. c) The capillary force induces the colloidal crystallization of the PS microspheres on the upper surface along with the infiltration of TiO$_2$ nanoparticles through the interstitial spaces. As water evaporation proceeds, the packing of PS microparticles is hampered by the increasing TiO$_2$ content and decreasing capillary force near the substrate, resulting in randomly packed arrays near the bottom of the composite film. However, higher volume occupation of TiO$_2$ nanoparticles at the bottom has a positive effect on the adhesion with the substrate and keeps the interface intact during thermal calcinations of the PS microspheres.

As shown in **Figure 2**, the surface charge of TiO$_2$ nanoparticles in aqueous dispersions with a pH value above 7 is stable at ~−42 mV, but it diminishes dramatically for a pH value below 7. The PS microspheres in a neutral pH medium also carried a negative surface charge of ~30 mV thanks to the sulfate groups incorporated into the nanoparticles during synthesis. Thus, a binary dispersion of PS and TiO$_2$ with a pH value above 7 was
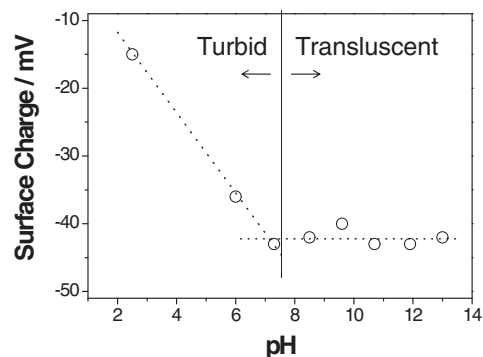
Figure 2. Surface charge of TiO$_2$ nanoparticles vs. pH variation. As the aqueous medium becomes acidic, the surface charge of TiO$_2$ decreases due to the protonation of the surface hydroxyl groups, and the solution turns turbid as a result of the nanoparticles coagulation.

maintained stable for several weeks without visible signs of clogging.

The TiO$_2$ dispersion mixed with a low pH buffer was found to become turbid right after mixing. This is because the surface charge of TiO$_2$ nanoparticles decreased due to the protonation of surface Ti–OH groups, the electrostatic repulsion between them diminishes and, finally, the dispersion is coagulated. In the present study, however, the pH of the binary mixture was maintained above 8 during the entire coating process. Thus, it is reasonable to suppose that no pH-driven coagulation of TiO$_2$ nanoparticles occurred, which could otherwise have resulted in randomly packed arrays of PS colloids. It should also be noted that the continuous evaporation of water during the coating process results in a gradual increase in the TiO$_2$ content of the binary mixture. Such an increase would hamper the diffusion of PS microspheres and consequently, their self-assembly. In addition, the strength of capillary forces decreases in the longitudinal direction of the substrate. As a consequence of the gradient in the TiO$_2$ concentration as well as in the strength of capillary forces, the bottom layers generally end up with a randomly packed structure unlike the well-ordered structure of the upper layers (see Figure 1c). The SEM images of the freeze-fractured TiO$_2$ IO film clearly show the random orientations of the PS microspheres at the bottom of the IO film as well as the highly ordered structure close to its surface. (**Figure 3**)

A 3D reconstructed image of the TiO$_2$ IO film is shown in Figure 3, along with an optical photograph and magnified SEM images of the surface and the cross section of the film. The TiO$_2$ IO film has a very shiny reflective surface as a result of its highly ordered colloidal crystal structure near the surface. Since PS microspheres are burned off during calcination, one can recognize their traces left in the form of spherical air cavities. Figure 3b,c show low and high magnification SEM images of the specimen's center region which is indicated by a small rectangle in Figure 3a. As shown in Figure 3b, the surface of the TiO$_2$ IO film exhibits predominantly hexagonal arrays of air cavities which correspond to {111} FCC layers parallel to the film surface. This distinguishing feature of the fabricated TiO$_2$ IO film resembles the film fabricated by Meng et al. who simultaneously assembled PS microspheres and TiO$_2$ nanoparticles following a procedure similar to the method presented in this paper.[12] However, this slow dip-coating method led to the formation of {100} parallel to the film's surface in majority.

Although further investigations are needed to determine the detailed mechanisms underlying the formation of layers with the preferred {111} orientation in this study, it can be attributed to the accelerated water evaporation from the film surface by hot air evenly blown on it, which is expected to promote the formation of close-packed hexagonal arrays of the particles at the surface, as well as of the close-packed FCC structure of the

www.MaterialsViews.com

ADVANCED
FUNCTIONAL
MATERIALS
www.afm-journal.de

FULL PAPER
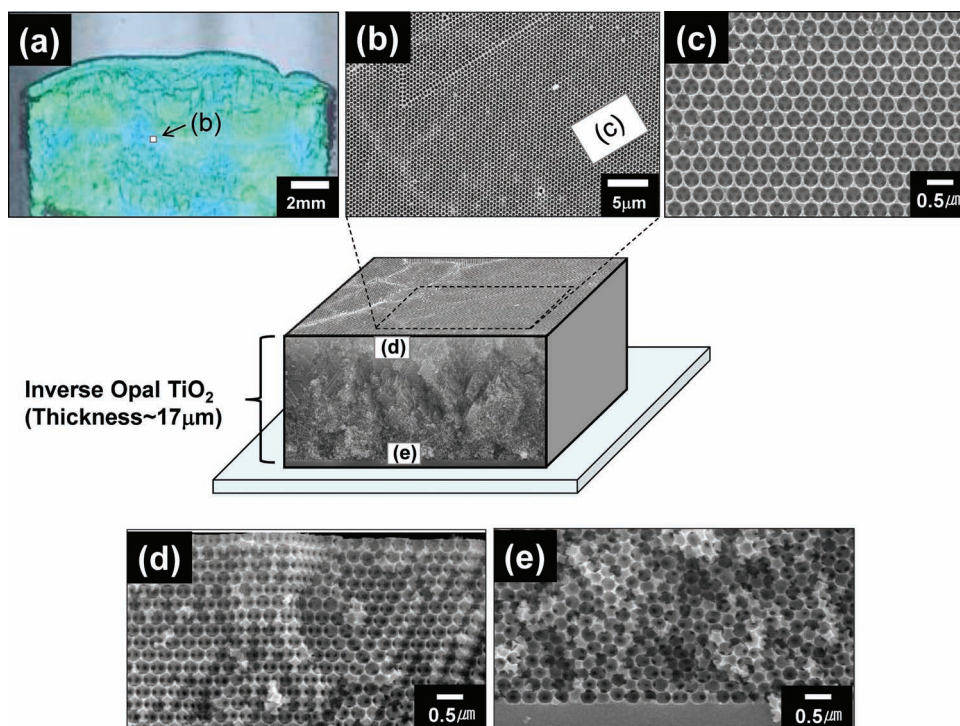
Figure 3. An optical photograph and the corresponding SEM images of the upper surface of the TiO$_2$ IO film deposited on a glass substrate using PS280 as sacrificial particles. (Coating rate: 1 mm min^{-1}.). Cross-sectional SEM images of the same TiO$_2$ IO film are also shown. The spots from which the SEM images are taken are indicated in the 3D reconstructed image at the center of the figures. It is clearly shown in (b) and (c) (top view) that the orientation of near the surface is exclusively {111} FCC. On the other hand, the cross-sectional images show that the top layers shown in (d) are well-ordered while bottom layers ((e)) are poorly ordered. Due to a relatively low packing density of sacrificial PS particles and high content of TiO$_2$ at the bottom, colloidal crystals are strongly adhered to the glass substrate.

underlying layers in an epitaxial manner. If the binary colloidal suspension is subject to a slow vertical coating under high humidity condition, the mechanism of colloidal assembly as well as the resulting morphologies can be altered.[12] As suggested by Norris and his colleagues, the "lateral solvent flow" at the drying front of the binary colloidal crystal could be responsible for the packing of particles which gives rise to the formation of a FCC structure rather than for the random hexagonal close packing (RHCP) that results from the mixed structures of FCC with HCP (hexagonal close packing) under the influence of niches through which the solvent is drawn and the following particle is deposited.[21] Solvent-driven colloidal crystallization can also be applied to our system. However, in our case, "the solvent" is actually the suspension of TiO$_2$ nanoparticles rather than a pure liquid.

Comparing the surface and the cross-section of the coated film, the as-coated binary colloidal crystal film was almost crack-free while thermal calcination at 450 °C produced some cracks along the surface of TiO$_2$ IO film (see Figure S2). Recently, Xu et al. reported that the lateral shirinkage of the 3D porous films after firing off the organic contents can be minimized since they are adhered to the substrate, while the shrinkage along the longitudinal direction would become even more substantial.[22] A dissimilarity between lateral shrinkage and that along the longitudinal direction will be discussed in a later section. It is noteworthy that, since our TiO$_2$ nanoparticles were hydrothermally treated and subsequently purified, the organic compound was

almost removed, and the lateral cracking as well as the longitudinal shrinkage of the sintered film was not as serious as that of previous report. By fabricating TiO$_2$ IO films using a wide variety of sacrificial PSs with different sizes, it was confirmed that the coating method first developed in this study allows for the formation of well ordered IO colloidal crystal films over a large area (~a few cm^2), and the cracks after the thermal calcination are minimized. (see the Supporting Information, Figure. S3 and S4)

Figure 3d and e show magnified images of the cross-section of a 17 μm thick TiO$_2$ IO film having a different degree of orientation near its upper surface and the substrate below. Although well-ordered FCC IO structures are dominant in the longitudinal direction, about one third of all bottom PSs are randomly packed. When larger PS microspheres are used as template, the thickness of randomly packed region generally increases due to the relatively slower mobility of larger PS microspheres in a fluid medium. However, it is noteworthy that the random packing of PS microparticles near the glass substrate can have a positive effect on the adhesion between the TiO$_2$ film and the substrate. Random orientation of the sacrificial particles translates into a higher volume fraction of TiO$_2$ than within a close-packed structure (e.g. for FCC lattice structures, the interstitial volume is estimated to be 26% and it increases as the ordering gets poorer), offering a larger contact area between the TiO$_2$ film and the substrate. The weakness of the infiltration-based TiO$_2$ IO film used as a photoelectrode for DSSCs is expected to

FULL PAPER

be the poor contact with the substrate which is directly related to the electron transport and the photon-to-current efficiency of the solar cell.[8] By sacrificing the well ordered structure at the bottom of the film, we gained a more important quality, mechanical robustness. Nevertheless, the binary suspension and the coating condition were optimized in the present investigation to minimize the thickness of disordered layers and thus to provide highly reflective photonic crystal film.

### 2.2. Optical and Mechanical Properties of the TiO₂ IO Film

The structural color of the IO film originates in the selective reflection of the ambient light at the {111} planes of FCC colloidal crystals. The center wavelength of the reflected light can be approximately estimated using the modified Bragg equation as follows:

$$\lambda_{max} = \left(\frac{8}{3}\right)^{1/2} \cdot \left(\frac{d}{m}\right) \cdot \left(f_1 \cdot n_1^2 + f_2 \cdot n_2^2 - \sin^2\theta\right)^{1/2}$$

$$= 1.633 \cdot \left(\frac{d}{m}\right) \cdot \left(f_1 \cdot n_1^2 + f_2 \cdot n_2^2\right)^{1/2}$$

$$= 1.633 \cdot \frac{d}{m} \cdot n_{eff},$$

assuming normal reflection $(\theta = 0)$ (1)

where, d is the diameter of the PS microsphere (or air cavities of the IO film), m is the order of the Bragg diffraction, n_1, n_2, f_1, f_2 are the refractive index and filling factor of the microparticle (or air cavities) and interstices, respectively, θ is the angle measured from the normal to the plane of the colloidal crystal film. The reflected color is often referred to as "structural color" since it is the ordered structure that is responsible for the selective light reflection.

For quantitative analyses of the relationship between the structural color and the film's characteristics, reflectance spectra of each film were obtained at every processing stage. In **Figure 4**, the reflectance spectra of a) the PS colloidal crystal film, b) the composite PS/TiO₂ film, and c) the final TiO₂ IO film using PS280 as the colloidal crystal template are shown. A bare PS colloidal crystal film was obtained by depositing only the PS280 emulsion on the glass substrate. In Figure 4, the SEM images of each film are also shown on top of each reflectance peak. In particular, the reflectance peak of the PS colloidal crystal film corresponds to the {111} Γ-L pseudogap (or stop band) of a FCC photonic crystal, and the peak maxima (λ_{max}) are mathematically related to the average diameter of the PS microspheres by the Bragg relation, as shown in Equation 1. Assuming that the reflectance originates in a perfect FCC {111} crystalline plane made of PS microspheres ($f_{PS} = 0.74$, $n_{PS} = 1.59$) and air cavities ($f_{air} = 0.26$, $n_{air} = 1.00$), n_{eff} would be equal to 1.46. According to Equation 1, the first order diffraction peak is expected to appear at a wavelength of 667 nm, while the experimentally observed λ_{max} is located at 635 nm (Figure 4a). About 5% of the discrepancy between the λ_{max} predicted and observed can be attributed to the presence of loosely packed colloidal arrays within the colloidal crystal film. To compare the reflection peak of the
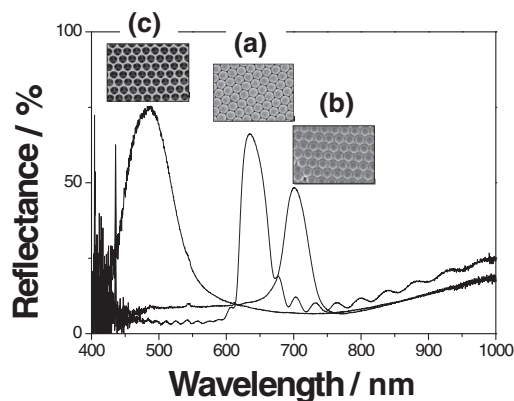
Figure 4. Reflectance spectra and SEM images of the colloidal crystal films using PS280 as template-forming particle. a) Colloidal crystal with PS microspheres only, b) composite PS/TiO₂ film, c) TiO₂ IO film after burning off the PSs of the composite film shown in (b) by thermal calcination.

composite TiO₂/PS colloidal film observed with the theoretically predicted value, n_{TiO2} was assumed to be equal to 2.0 in our calculations, which has been estimated for the thin TiO₂ film deposited on a silicon (Si) wafer by means of ellipsometry.[20] In the case where the n_{eff} of the composite film is 1.72, the wavelength λ_{max} corresponding to the reflection peak was calculated to be 787 nm. As shown in Figure 4b, the observed λ_{max} was 700 nm which is different from the expected value by 11%. This increased error is thought to be the consequence of the relatively small refractive index of the TiO₂ film due to incomplete drying, or differently, of air gaps between TiO₂ and PS microspheres which originate in the solvent evaporation and reduce the filling fraction of the high index material and eventually, the n_{eff}. In the case of the TiO₂ IO film, the calculation of the λ_{max} after the thermal calcinations revealed an even larger difference from the observed λ_{max}. Before proceeding to more details about the result of these calculations, it is necessary to consider the lateral shrinkage of the film by comparing interparticle distances before and after the thermal calcinations. For the films made of PS microspheres of different sizes, the shrinkage in the interparticle distance was estimated to be 3~6%. (see the Supporting Information, Table S1.) When compared to the 1-dimensional shrinkage which was estimated to be ~10% in our previous study, the present method offered an outstanding improvement from the view point of shrinkage.[9] The improved lateral shrinkage can be attributed to the successful removal of all organic compounds from TiO₂ suspension (e.g. TMAH) at the final stage of TiO₂ synthesis. However, desorption of the residual water molecule from the TiO₂ should have exerted inevitable degree of shrinkage to the film. Thus, approximately 5% of the shrinkage along the longitudinal direction was also taken into account in the pore size analyses. Furthermore, we considered the increase in the refractive index of TiO₂ (n_{TiO2} ~2.3) which originates in thermal sintering. The calculated λ_{max} was 629 nm (= 1.633 × 280 nm × 0.95 × 1.45), while the λ_{max} observed was 485 nm (23% discrepancy). As addressed in the previous report, we attributed the lower than predicted λ_{max} to the dissimilarity of the lateral and longitudinal shrinkage.[22] A

(a)
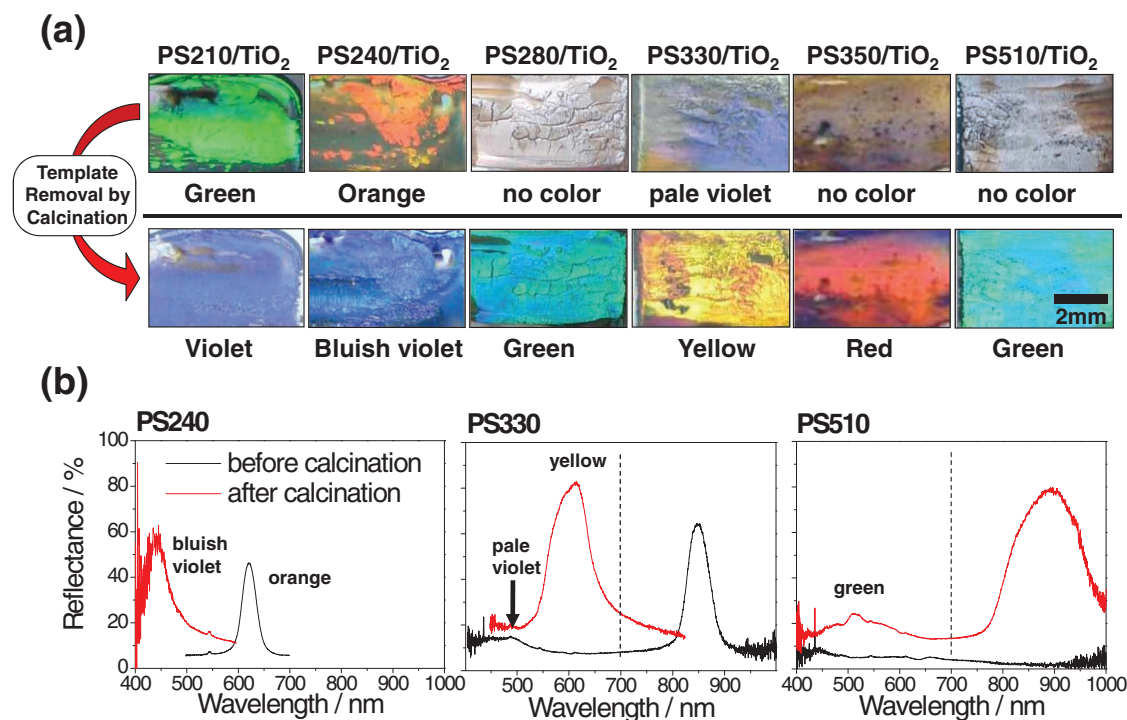
Figure 5. a) Optical photographs of the composite PS/TiO$_2$ films templated by differently sized PS microspheres and the corresponding TiO$_2$ IO films after calcination. b) Three reflectance spectra selected from the films shown in the photographs. Dashed line in the reflectance spectra indicates the limit of visible range (700 nm) over which the peak does not correspond to a structural color. Since PS templates are burned off by thermal calcinations that alter the optical characteristics such as the refractive indices and the size of the periodic structures, the color of the films and their spectra also changes. The wavelength of the reflected light at four TiO$_2$ IO films is defined by the first order Bragg diffraction of light at the respective IO structure, while the green color of the TiO$_2$ IO film templated by PS510 microspheres originates in the second order diffraction, as shown in the reflectance spectra shown in (b).

closer look at Figure 3d and e reveals that air cavities viewed from the cross-section of IO structure are approximately elliptically shaped, compared to the spherical air cavities shown in Figure 3c (the IO film viewed from above). Since the film is in contact with the glass substrate which maintains its dimensions during thermal treatment, the volume contraction of the TiO$_2$ film is more pronounced in the longitudinal rather than the lateral direction.[22] In SEM images of the cross-section of other IO films, we identified partially flattened air cavities along the longitudinal direction which is in agreement with the previously given explanation. (for further information, see the Supporting Information, Figure S5) The increasing discrepancies between the theoretically predicted and experimentally observed λ_{max} with the PS/Air, PS/TiO$_2$, and Air/TiO$_2$ structures were confirmed by comparing the reflectance spectra of these three films made of different PS microspheres (PS240 and PS330). Nevertheless, Figure 4 clearly shows the high reflectance (~75%) as well as the wide stop band of the TiO$_2$ IO film which can be attributed to a high index contrast between air and TiO$_2$ (1.0 vs. 2.3). Despite high reflectance and the clear structural color from entire colloidal films shown in Figure 3(a), there exist inevitable defects and crystal grains within the film since the slide coating relies on the self-assembly process of the colloids. The heterogeneity of the film was not serious though, and it could be confirmed by comparing the reflectance spectra from various spots which showed less than 5% variation of λ_{max}. (Figure S6)

For the IO film shown in Figure 3, the average thickness was estimated to be equal to ~17 μm, when the coating speed is 1 mm min^{-1}. Under a similar solid content and weight ratio for the PS microspheres and TiO$_2$ nanoparticles in the binary mixture, the thickness of the coated film was found to be dependent only on the coating speed (pulling rate of the top cell), regardless of the PS microsphere size. As expected, the thickness of the TiO$_2$ IO film was inversely proportional to the coating speed. (see the Supporting Information, Figure S5 and S7)

In **Figure 5**a, the photographs of six different films fabricated using different PS microspheres as template are shown. The next step was to compare the photographs taken before and after thermal calcination of each film, which appear to have different colors depending on the wavelengths covered by photonic stop band. Before the template was removed, only the color of the films fabricated from PS210 (green), PS240 (orange), and PS330 (pale violet) could be distinguished. The colors of the TiO$_2$ IO films, on the other hand, spanned from violet to red, as the diameter of the PS microspheres increased from 210 nm to 350 nm. As PS size reached a value as high as 510 nm, the reflection maxima from the composite film was not observed within the range of wavelengths covered by our measurement instruments (black baseline in the third reflectance spectra in Figure 5b). After calcinations, however, reflection maxima at the wavelength ~900 nm is observed which is
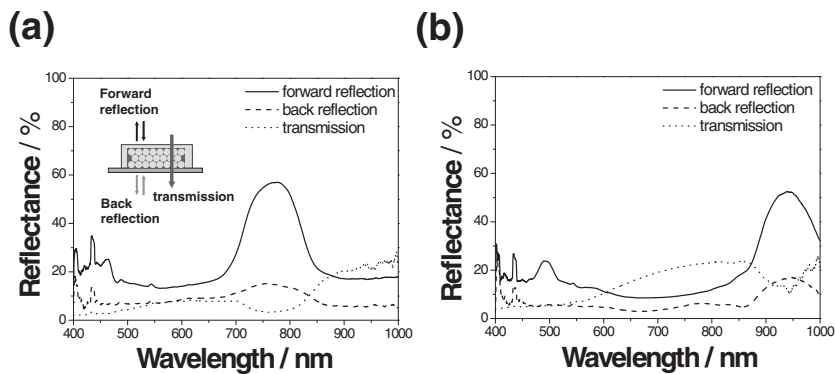
Figure 6. Transmission and refectance spectra measured from the both sides of the titania inverse opal film with a) air, and b) acetonitrile in the interstitial spaces. The 10 μm thick film was deposited on glass substrate, and PS450 was used as the sacrificial PS colloidal template.

a stop band at 780 nm with more than 50% peak reflectance for air/TiO_2 structure. However, the reflection from the back (substrate) side showed very small stop band peak due to the disordered pore structure. According to those reflectances, transmission was measured to be very low throughout the visible wavelength region, only showing a shallow stop band dip near 780 nm. The transmitted light intensity was a bit enhanced by infiltrating the IO structure with acetonitrile which is a common solvent for the electrolyte system used for DSSC as shown in Figure 6b. Owing to the increase in n_{eff}, the stop band positions of both reflections and transmission spectra were red-shifted to 940 nm from 780 nm.

in near-IR range. Although the diffraction of a 900 nm light cannot be recognized by human eyes, the second order Bragg diffraction was strong enough to show green color being diffracted by the TiO_2 IO film, something that is also evident from the diffraction peak. By plotting the reflection maxima (λ_{max}) for all the TiO_2 IO films fabricated with sacrificial PS microspheres of different sizes, the linear relationship between the λ_{max} and the diameter of PS microspheres, which can be easily derived from the Bragg equation, was confirmed. (for further details see the Supporting Information, Figure S8)

Since the TiO_2 IO films obtained in this study exhibit highly ordered FCC {111} layers parallel to the surface and disordered layers near the substrate, the reflectance spectra measured from two sides appeared differently. In **Figure 6**a, three different spectra from a air/TiO_2 IO film (templated by PS450 sacrificial particles) are shown. Just as shown in the previous examples, forward reflection (measured from the film surface) showed

As mentioned earlier, the TiO_2 dispersion used in this study underwent hydrothermal treatment before it was mixed with PS microparticles. Therefore, we examined the effect that the hydrothermal treatment has on the quality of the final TiO_2 IO films. For this test, two different binary mixtures were prepared. The first mixture contained PS280 and TiO_2 nanoparticles and did not undergo any hydrothermal treatment. Since anatase TiO_2 nanoparticles are formed after the peptization process, the mixture looked almost the same as the usual binary mixture. Still, it differed in the TiO_2 particle size (~8 nm) which is smaller than that of hydrothermally treated TiO_2 (~20 nm). The second aqueous mixture with the same solid content was composed of PS280 microspheres and hydrothermally treated TiO_2 nanoparticles. Each mixture was deposited on a glass substrate at the same coating speed to obtain film of approximately the same thickness and subsequently, calcined. In **Figure 7**a, b, and c, the SEM
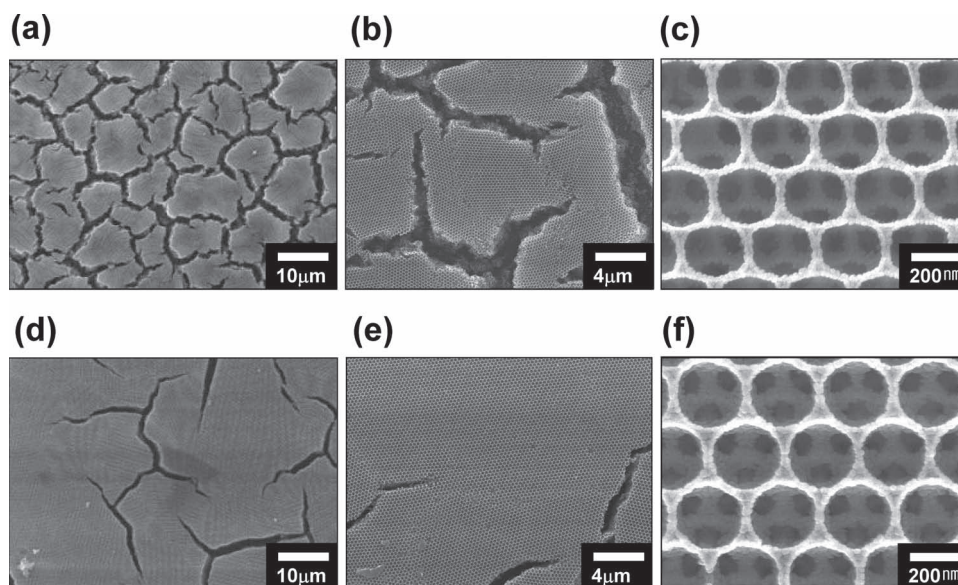
Figure 7. SEM images of TiO_2 IO films fabricated using the same PS template (PS280) microspheres, total solid content, and the coating speed (1 mm/min), but different TiO_2 nanoparticles showing the importance of hydrothermal treatment of TiO_2. a–c) SEM top view images of the TiO_2 IO film made from TiO_2 nanoparticles without hydrothermal treatment. d–f) Images of a TiO_2 IO film prepared using hydrothermally treated TiO_2 nanoparticles.

www.MaterialsViews.com

ADVANCED
FUNCTIONAL
MATERIALS
www.afm-journal.de

FULL PAPER

(a)

(b)
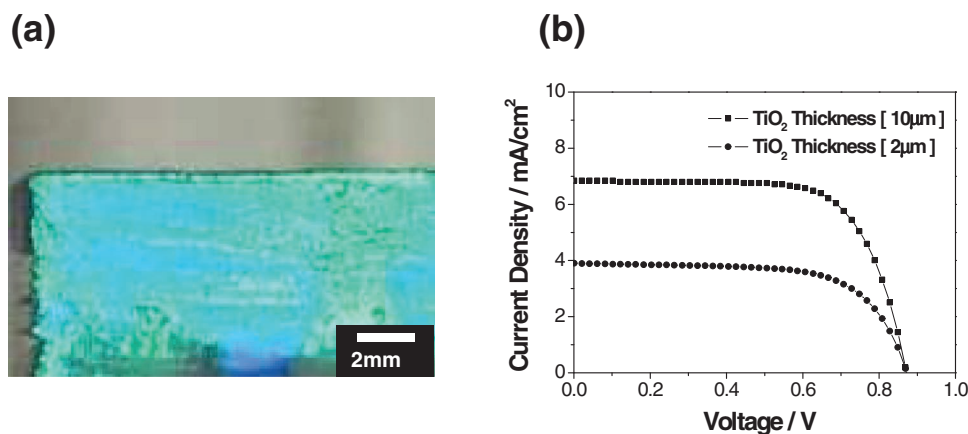
Figure 8. a) Optical Photograph of the FTO glass substrate on which the preformed TiO$_2$ blocking layer is coated. PS510 and 1 h hydrothermally treated TiO$_2$ was used to prepare the binary mixture. b) Typical I–V characteristics of single DSSCs made of TiO$_2$ IO photoelectrodes deposited on a FTO substrate with different thicknesses.

images of the TiO$_2$ IO films fabricated using TiO$_2$ nanoparticles without hydrothermal treatment which were taken from above, are shown. The significantly large number of cracks observed is due to the substantial volume shrinkage during calcination. As shown in Figure 7c, relatively large air cavities and their deformed shape provide evidence of substantial volume shrinkage. On the contrary, the thin films prepared based on hydrothermally treated TiO$_2$ nanoparticles showed a significantly reduced number of cracks, as shown in the SEM images of Figure 7d, e, and f. By comparing the magnified SEM images of each film (Figure 7c and f), we concluded that the use of hydrothermally treated TiO$_2$ resulted in TiO$_2$ nanoparticles and IO cavities of relatively larger sizes, but smaller connecting holes in an IO film which evidently underwent less serious volume contraction.

2.3. TiO$_2$ IO Films Used as DSSC Photoelectrodes

To verify the advantageous features of TiO$_2$ IO film (eg. hight porosity, high TiO$_2$ content, good interfacial contact with the substrate) fabricated in this study, the film was tested as an electrode for solar cell. By means of the method described in this paper for the fabrication of TiO$_2$ IO films, a DSSC photoelectrode was prepared. In other words, we followed the same fabrication path for a standard single DSSC as in our previous study, but the photoelectrode was prepared differently.[9]

To obtain the photoelectrode, an aqueous dispersion of binary PS510/TiO$_2$ mixture was deposited on an FTO glass substrate. In the current investigation, we chose a large sized sacrificial PS to avoid photonic bandgap effect from the photonic crystal structure of TiO$_2$ IO film, which will be dealt in the following study. By increasing the coating rate from 1 mm min^{-1} to 3 mm min^{-1}, a 10 μm and a 2 μm thick film were prepared. (for further details see the Supporting Information, Figure S9) Both films deposited on a FTO glass were not only as robust as those deposited on a slide glass, but they could also be directly immersed in a dye solution and subsequently, dried.

The assembly of a dye-doped photoelectrode with a counter electrode, and infiltration of the electrolyte would complete the preparation of a single DSSC. **Figure 8**b shows the typical I–V characteristics of two single DSSCs with a TiO$_2$ IO photoelectrode of different thicknesses under the irradiance of AM 1.5G sunlight shining from the photoelectrode side. As expected, the thicker the photoelectrode was, the higher the light-to-electricity conversion efficiency of a single solar would be (4.16 vs. 2.23%). The related photocurrent–voltage characteristics are summarized in **Table 1**. Despite the simplicity of the fabrication procedure followed for the photoelectrodes, the light-to-electricity conversion efficiency, η, was doubled compared to that reported in our previous paper.[9] More specifically, with a TiO$_2$ film of approximately the same thickness and cavity size (12 μm and 400 nm, respectively), the efficiency previously attained did not exceed 2.86%. It is noteworthy that only a 2 μm thick TiO$_2$ film exhibited efficiency comparable to that of a 12 μm thick electrode prepared in our previous study. The improvement in the solar cell performance can be attributed to the distinct source of TiO$_2$ nanoparticles as well as to the modified preparation procedure. First of all, the volume shrinkage of TiO$_2$ nanoparticles upon thermal calcinations has been minimized. In our previous study, the TiO$_2$ nanoparticles were organically modified to achieve a higher level of dispersibility in the organic solvent. Although with well dispersed TiO$_2$ nanoparticles exhibited, high degree of infiltration could be attained within the polymeric template, the volume contraction due to the loss of organic modifiers during calcination could not be surpassed.

Table 1. Photocurrent-voltage characteristics of TiO$_2$ IO solar cells.

TiO$_2$ Film Thickness [μm]	Active area [cm^2]	V_{oc} [V]	J_{sc} [mA cm^{-2}]	FF [%]	η [%]
10	0.222	0.871	6.85	69.63	4.16
2	0.222	0.862	3.90	66.40	2.23

V_{OC}: Open circuit voltage. J_{SC}: Short circuit current. FF: Fill factor. η: Light-to-electricity conversion efficiency.

FULL PAPER

In this paper, the stability of the TiO$_2$ nanoparticle system originated in the pH-driven coulombic repulsion among the nanoparticles. On the other hand, the volume contraction was mostly due to loss of initially adsorbed water molecules and furthermore, unlike in the case of an organic modifier, it could be minimized. The less contracted TiO$_2$ films deposited on the FTO substrate allowed us to easily achieve electron transport through the highly interconnected TiO$_2$ network as well as a larger cell area. Secondly, the coating method described in this paper ensures a higher TiO$_2$ content in a photoelectrode, which induces the higher loading of dye molecule and a better interfacial contact between the TiO$_2$ film and the FTO glass. Unlike the successive infiltration-drying steps of the previous method, in which the TiO$_2$ nanoparticles might not be transported all the way to the bottom of the template (which is true for many occasions), the newly developed method consists of just one step during which the TiO$_2$ nanoparticles are mixed with the template-forming PS microspheres and at the same time deposited on a glass substrate. The TiO$_2$ nanoparticle content of the final film can reach values as high as 26% (i.e., the maximum content in a FCC structure) and facilitate the adsorption of dye molecules. Moreover, it is inherently free from a "infiltration to the bottom" problem. The TiO$_2$ content in the vicinity of the FTO glass substrate is higher than near the upper surface due to the non-close-packed sacrificial particles. Assuming that the volume contraction of TiO$_2$ is not sufficient to generate cracks at the interface, there should be enough pathways for the electrons at the interface to be transferred to the FTO electrode. More rigorous DSSC investigations have already been planned which entail variations of sacrificial particle sizes, pH of the binary mixture that will allow us to control the orientation of sacrificial particles, etc.

Besides the usefulness as the photoelectrode of DSSC, the facile fabrication technique and the functional TiO$_2$ IO films presented in this study are expected to find many other applications such as dielectric reflectors for micro-laser and sensors since the films exhibit high reflectance provided by preferred {111} planes at the surface layers. Further improvement of the detailed slide coating processes and development of useful pair of microspheres and other inorganic nanoparticle systems will be the prerequisite for successful utilization of the technique.

3. Conclusions

A novel method for the fabrication of IO TiO$_2$ thin films has been successfully developed. The fabrication method is based on depositing a binary aqueous mixture of TiO$_2$ nanoparticles and PS microspheres directly on a glass substrate. Assisted by a flow of hot air accelerating the capillary force driven self-assembly of microparticles, it allows for the relatively quick and easy fabrication of mesoporous TiO$_2$ thin films. After firing off the sacrificial microparticles, the structure of the TiO$_2$ IO film was characterized with the aim to reveal the highly ordered FCC structures near the film's upper surface and randomly oriented bottom layers which are formed by the kinetically trapped microparticles upon water evaporation. Through the deposition of the binary mixture on a FTO glass followed by thermal calcination, DSSC photoelectrodes were fabricated and subsequently, attached to a DSSC. The photon-to-current conversion efficiency measured on a 10 μm-thick TiO$_2$ IO electrode was as high as 4.2%, which is improved by ~80% compared to recently fabricated IO electrodes.

4. Experimental Section

Materials: The monodisperse PS particles were synthesized by controlled emulsion polymerization following the same experimental procedure reported elsewhere.[23] By using different amount of surfactants, 7 PS microspheres with different particle sizes were obtained. (The sample code for PS particles stands for the average diameter in nanometer, such as PS210, PS240, PS280, PS330, PS350, PS450 and PS510.) All the PS microparticles showed narrow size distribution (<5%), and the particle sizes were characterized from SEM analyses. The PS content in an aqeous dispersion was ca. 10 wt%. Anatase TiO$_2$ nanoparticles were synthesized by peptization method followed by mild hydrothermal treatment as reported previously.[20] As a brief synthetic procedure, 3mL of Titanium isopropoxide (Ti(i-PrO)$_4$, TCI) wais slowly added to deionized (DI) water. After 1 hour or condensation reaction, crude product was rinsed with DI water at least for 3 times. Wet TiO$_2$ cake was mixed with 15mL DI water, and after addition of 1mL of tetramethylammonium hydroxide (TMAH) (ca. 25% in Water, TCI), peptization was carried out for 24 h at 85 °C. The obtained transluscent dispersion was further treated by mild hydrothermal process in a pressurized reactor (4744, Parr instruments) at 200 °C for 1 hour.[20] The product was sedimented by ultracentrifugation at 12 000 rpm, and washed with DI water twice for the remaining organic impurities to be eliminated. The final aqueous dispersion typically contained 5 wt% of TiO$_2$ nanoparticles which exhibited pH of 8~10. To test pH-dependent stability of the TiO$_2$ nanoparticles, the dispersion was diluted with excess amount of water in which different amount of TMAH and aqueous HCl mixed for pH adjustment. The turbidity and the surface charge of each dispersion at various pH were monitored.

Fabrication of TiO$_2$ IO Structure: As schematically shown in Figure 1a, a similar apparatus as previously reported was used for coating PS/TiO$_2$ hybrid films.[24] A slide glass (2.5 cm × 5.0cm) for bottom substrate was cleaned using Piranha solution (H$_2$SO$_4$: H$_2$O$_2$ = 3:1 by volume) and DI water prior to use. A half-cut slide glass was immersed in 1mM Trichlorooctadecylsilane dissolved in 2,2,4-Trimethylpentane (Jusei) for 30 min to render it hydrophobic. Fabrication of a top cell was completed by bonding a glass tube (length = 30mm, diameter = 5mm) to a drilled hole on a hydrophobic slide glass using epoxy resin (Hardex). The scotch tapes were cut and attached at both sides of the substrate with a desired thickness (typically 100 μm) in order to provide a thin space between a top cell and a sbstrate. Equal volumes of respective PS and TiO$_2$ dispersions were mixed, and about 300 μL aliquot of the mixed dispersion was gently introduced through the glass tube so that the dispersion can be infiltrated between the top cell and the substrate by capillary force. The top cell was then pulled by syringe pump (KD scientific) with a line velocity of 0.5–3.0 mm min^{-1}, depending on the desired film thickness. Colloidal self-assembly took place at the drying meniscus as shown in Figure 1b while hot air was blown from the top to accelerate water evaporation. Once the dispersion was converted to the hybrid colloidal assembly, the substrate with the hybrid film was subjected to the thermal calcinations at 300 °C for 2 h and 450 °C for 2 h respectively in a furnace (heating rate = 2 °C min^{-1} to remove PS particles. (Figure 1(c)).

DSSC Single Cell Test: On a clean FTO glass (TEC-8, Pilkington), 7% 1-butanol solution of Titanium(IV) bis(ethyl acetoacetato)-diisopropoxide solution (Aldrich) was spin coated, and the coated precursor film was thermally calcined at 450 °C to form a thin TiO$_2$ blocking layer. Using that as a bottom substrate, the TiO$_2$ IO photoelectrode was fabricated following the same procedure as described elsewhere.[9] The TiO$_2$ photoelectrode was immersed in 0.5 mM N719 dye (cis-bis(isothiocyanato)-bis(2,20-bipyridyl-4,40-dicarboxylate)

www.MaterialsViews.com

ADVANCED
FUNCTIONAL
MATERIALS
www.afm-journal.de

FULL PAPER

ruthenium(II) bis (tetrabutylammonium), solaronix) in ethanol for 1 day. The excess dye was washed away with ethanol. Pt counter electrode was fabricated by spin coating 0.7 mM H_2PtCl_6 in 2-propanol on an FTO glass followed by thermal sintering at 450 °C for 2 h. A photoelectrode and a Pt counter electrode were sandwiched using 25 μm Surlyn® sheet (1702 DuPont) as spacer. Liquid electrolyte was gently inserted through a hole at the counter electrode, and the single cell was completed by sealing the hole with Surlyn. The liquid electrolyte used in this study was composed of 0.7 M 1-butyl-3-methylimidazolium iodide (BMII), 0.03 M Iodine (I_2), 0.1 M Guanidium thiocyanate (GSCN), and 0.5 M 4-tert-butylpyridine (TBP) in a mixed solvent of acetonitrile and valeronitrile by 85:15 volume ratio. Photocurrent was measured using a source measuring unit (model 2400, Keithley) under AM 1.5 G one-sun condition. The data was compared with that of NREL-calibrated Si solar sell.

Characterizations: Morphologies of PS colloidal particles and TiO_2 IO films were characterized using a field-emission scanning electron microscope (FE-SEM, Hitachi S-4700). Reflectance spectra from the photonic crystal films before and after calcinations were obtained using a fiber optic UV-Vis spectrometer (AvaSpec, Avantes) which was coupled to an optical microscope (Bimeince) with halogen lamp as light source. Using a microscope objective lens (20x, N.A. = 0.3), nearly specular reflectance was collected from ~1mm² area of the colloidal crystal.

Supporting Information

Supporting Information is available from the Wiley Online Library or from the author.

Acknowledgements

[1] A. L. Linsebigler, G. Q. Lu, J. T. Yates, *Chem. Rev.* **1995**, *95*, 735.
[2] C. Wang, Z.-X. Deng, Y. Li, *Inorg. Chem.* **2001**, *40*, 5210.
[3] I. Moriguchi, H. Maeda, Y. Teraoka, S. Kaawa, *Chem. Mater.* **1997**, *9*, 1050.
[4] S. D. Burnside, V. Shklover, C. Barbe, P. Comte, F. Arendse, K. Brooks, M. Gratzel, *Chem. Mater.* **1998**, *10*, 2419.
[5] A. Fujishima, N. T. Rao, D. A. Tryk, *Electrochim. Acta.* **2000**, *45*, 4683.
[6] A. Kay, M. Gratzel, *Sol. Energy Mater. Sol. Cells* **1996**, *44*, 99.
[7] M. Gratzel, *Inorg. Chem.* **2005**, *44*, 6841.
[8] S. Nishimura, N. Abrams, B. A. Lewis, L. I. Halaoui, T. E. Mallouk, K. D. Benkstein, J. van de Lagemaat, A. J. Frank, *J. Amer. Chem. Soc.* **2003**, *125*, 6306.
[9] E. S. Kwak, W. Lee, N. G. Park, J. Kim, H. Lee, *Adv. Func. Mater.* **2009**, *19*, 1093.
[10] S. Jeon, P. V. Braun, *Chem. Mater.* **2003**, *15*, 1256.
[11] G. Subramania, K. Constant, R. Biswas, M. M. Sigalas, K. M. Ho, *Adv. Mater.* **2001**, *13*, 443.
[12] Q. B. Meng, C. H. Fu, Y. Einaga, Z. Z. Gu, A. Fujishima, O. Sato, *Chem. Mater.* **2002**, *14*, 83.
[13] J. D. Joannopoulos, R. D. Meade, J. N. Winn, in *Photonic Crystals: Molding the Flow of Light*, Princeton University Press, Princeton **1995**.
[14] O. D. Velev, E. W. Kaler, *Adv. Mater.* **2000**, *12*, 531.
[15] P. Jiang, J. F. Bertone, V. L. Colvin, *Science* **2001**, *291*, 453.
[16] R. C. Schroden, M. Al-Daous, C. F. Blanford, A. Stein, *Chem. Mater.* **2002**, *14*, 3305.
[17] J. H. Moon, Y. Xu, Y. Dan, S. M. Yang, A. T. Johnson, S. Yang, *Adv. Mater.* **2007**, *19*, 1510.
[18] Y. Xu, X Zhu, Y Dan, J. H. Moon, V. W. Chen, A. T. Johnson, J. W. Perry, S. Yang, *Chem. Mater.* **2008**, *20*, 1816.
[19] S. Guldin, S. Huttner, M. Kolle, M. E. Welland, P. Muller-Buschbaum, R. H. Friend, U. Steiner, N. Tetreault, *Nano Letters* **2010**, *10*, 2303.
[20] Y. G. Seo, H. Lee, K. Kim, W. Lee, *Mol. Cryst. Liq. Cryst.* **2010**, *520*, 201.
[21] D. J. Norris, E. G. Arlinghaus, L. Meng, R. Heiny, L. E. Scriven, *Adv. Mater.* **2004**, *16*, 1393.
[22] Y. Xu, X Zhu, S. Yang, *ACS Nano* **2009**, *3*, 3251.
[23] S. Kim, Y. G. Seo, Y. Cho, J. Shin, S. C. Gil, W. Lee, *Bull. Kor. Chem. Soc.* **2010**, *31*, 1891.
[24] S. C. Gil, Y. G. Seo, S. Kim, J. Shin, W. Lee, *Thin Solid Films* **2010**, *518*, 5731.